WALSEMA during PS131: Water vapor, cloud liquid water and surface emissivity

AUTHORS

Institute of Environmental Physics, University of Bremen | Bremen, Germany
J. Rückert, G. Spreen

Institute for Geophysics and Meteorology, University of Cologne | Cologne, Germany
K. Ebell, M. Mech, A. Walbröl

TEXT OF EXTENDED ABSTRACT (POSTER)

Measurement setup

The WALSEMA "Water Vapour, Cloud Liquid Water, and Surface Emissivity over the Arctic Marginal Ice Zone in Summer" project was a secondary user project during the ATWAICE (PS131) campaign from June to August 2022. Two microwave radiometers were installed on Polarstern's Peildeck: MiRAC-P (Microwave Radiometer for Arctic Clouds – Passive) (Mech et al. 2019) observing at high-frequencies (six channels around 183.31 GHz and two window channels centered at 243 and 340 GHz) and HATPRO (Humidity and Temperature Profiler), with seven channels each at K-band and V-band (Rose et al. 2005). In addition, a visual and an infrared (IR) camera facing the surface were installed next to the radiometers. Rotatable mirrors were attached to the radiometer stand to allow measurements towards the atmosphere and the surface. A sky camera (visual and IR) was complementing the microwave measurements. The setup is displayed in Figure 1.

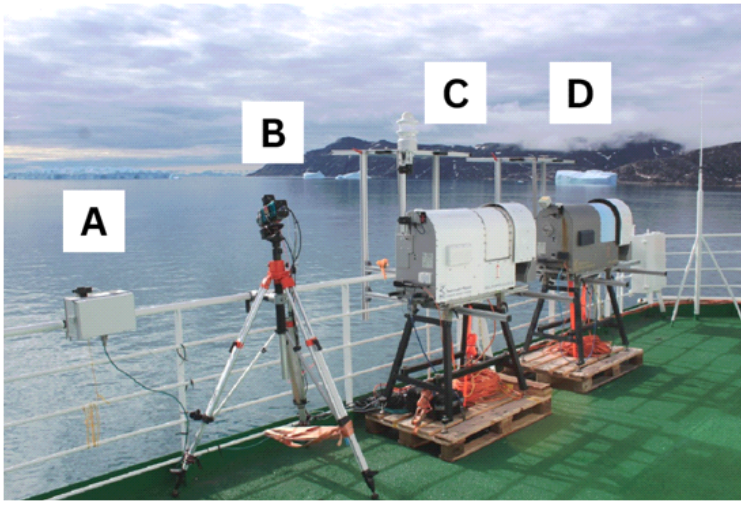

Figure 1: WALSEMA measurement setup during PS131 with (A) Sky camera, (B) IR surface camera with VIS surface camera on top, (C) MiRAC-P, and (D) HATPRO

Atmospheric observations: water vapor and cloud liquid water

Most of the time the radiometers pointed in zenith direction. From these observations vertical profiles of temperature and humidity, as well as liquid water path (LWP) and

integrated water vapor (IWV) were derived (Walbröl et al. 2022). Figure 2 shows the errors of the retrieved IWV as well as temperatue and humidity profiles with respect to the radiosondes launched during ATWAICE. The excellent agreement of the IWV with a root mean squared error (RMSE) of 0.46 kg m^{-2} and biases of only 0.15 kg m^{-2} demonstrates the high quality of the data. For the temperature profiles, we merged zenith and boundary layer scan observations to improve the vertical resolution in the boundary layer. The comparison to the radiosondes shows relatively small errors of 1-2 K in the lower troposphere despite the presence of strong temperature inversions, which are difficult to resolve with passive microwave observations. Temperature biases are also mainly between -1 and +1 K. The retrieved absolute humidity (ρ_v) profiles have relative RMSE (normalized by the radiosonde data) of about 20 % in the lower and up to 50 % in the upper troposphere.

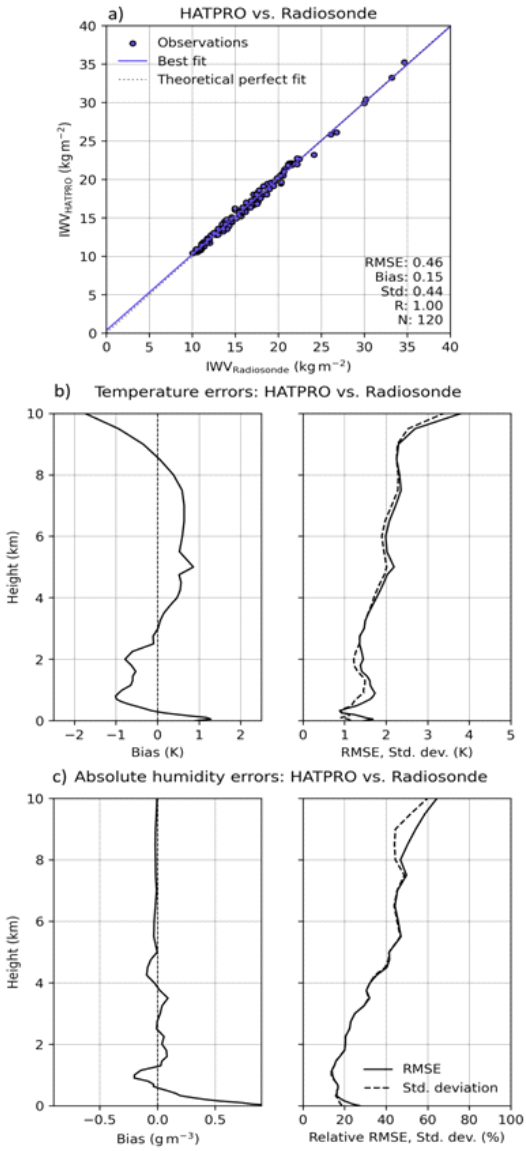

Figure 2: Comparison between meteorological observations (integrated water vapor, temperature profiles and humidity profiles) from radiosondes and microwave from radiometer data. In a) we show a scatterplot of integrated water vapor (IWV) from the radiosonde data vs the collocated IWV derived from the radiometer data. Differences in temperature profile (b) and absolut humidity profile (c) are shown as bias and root mean square error (RSME) in the other two panels.

The most notable event recorded with these atmospheric measurements is a series of two warm and moist air intrusion that occurred from 15-17 July and 17-19 July.

Significant and untypically high moisture (IWV of 35 kg m^{-2}) and temperatures up to 18°C at 650 m altitude were recorded at Polarstern, which was residing on the lee side of Svalbard at that time (see Fig. 3). The LWP, derived with an uncertainty of approximately 20 g m^{-2}, shows the highly variable cloud conditions encountered during PS131. During the warm air intrusions, the LWP varied between 0 and 350 g m^{-2}.

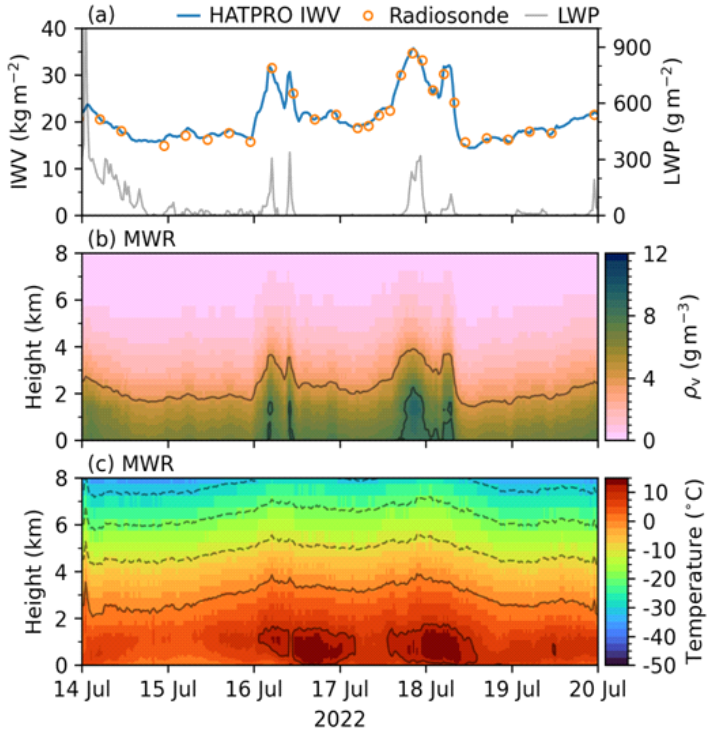

Figure 3: Measurements of integrated water vapor (IWV) and liquid water path (LWP) (a), humidity (b) and temperature profiles (c) from the microwave radiometers. In addition, IWV from radiosondes is shown in a). Shown is the time period around the two warm air intrusions.

Surface observations: Microwave emissivity

In addition to the atmospheric observations, the mirror construction enabled us to point at the surface. Since the cruise was conducted in the melting season, the physical temperatures of the encountered ocean, (bare) ice, and melt pond surfaces were similar and thus changes in the measured microwave brightness temperatures can be mainly attributed to changes in emissivity. The surface observations were done on a regular basis each hour at a viewing angle of 53° for 15 minutes. Note that the measured brightness temperatures have frequency-dependent polarizations. The surface was also scanned at various zenith angles five times during the cruise when the mirror was rotated manually.owever, due to the heterogeneous ice surface (melt ponds, leads, bare ice), which changes with incidence angle, the angle-dependence analysis is not conclusive.

The measured microwave brightness temperatures at 53° show distinct signatures for different surface types in the marginal ice zone at the low frequencies between 22 and 31 GHz, where it can be assumed that the atmosphere does not dominate the signal.

Brightness temperatures are around 160 K for open water and around 260 K for ice observations. At 51.26 and 52.28 GHz a contrast between sea ice and open water is observed as well. No distinction between ocean and sea ice was identified for the other frequencies in the 58 GHz oxygen absorption complex. Here, the atmospheric

contributions dominate the signal and the signals correspond to the air temperatures. Similarly, no distinct surface signal could be identified at the frequencies along the 183 GHz water vapor line where the atmospheric contributions caused by water vapor are dominating and the signals correspond to integrated water vapor values. At 243 GHz, the atmospheric moisture has a stronger influence than between 22 and 31 GHz but is not dominating the signal and the surface again is the main contributor. But because of the stronger moisture influence, the ice and ocean have less distinct emission signatures than at frequencies between 22 and 31 GHz.

Using the collocated skin temperatures derived from the infrared camera observations and the down-welling atmospheric contributions derived from the zenith observations, microwave emissivities for all measured frequencies and (pseudo-)polarizations were calculated. One example for 22.24 GHz, where the distinction between open ocean and sea ice is evident, is shown in Figure 3. Here, microwave measurements were collocated with the visual images and it was found, that high emissivities correspond to sea ice (high red-blue (R-B) ratio in the visual camera), while low emissivities correspond to open water (low R-B ratio). Emissivities at 22-31 GHz (predominantly vertically-polarized) between 0.51 ± 0.01 and 0.55 ± 0.01 for open ocean and around 0.95 ± 0.02 for sea ice were derived. At 243 GHz (predominantly horizontally-polarized) the distinction is less pronounced: ice surfaces exhibit a large variability with values around 0.67 ± 0.04 and around 0.83 ± 0.04. Ocean emissivities at this frequency are around 0.78 ± 0.01. The results shown can improve the characterization of surface emissions in satellite retrieval algorithms. More details on the surface microwave emissivity observations can be found in Rückert et al., 2025.

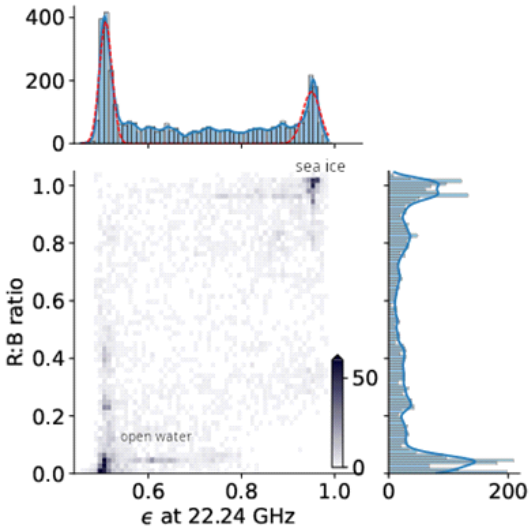

Figure 4: Emissivity ε at 22.24 GHz co-located with the ratio of red (R) to blue (B) from the RGB images of the visual camera. Shown are bivariate and marginal histograms with kernel density estimates (blue line).

REFERENCE

Mech M, Kliesch LL, Anhäuser A, Rose T, Kollias P and Crewell S. Microwave radar/radiometer for Arctic clouds (MiRAC): First insights from the ACLOUD campaign, *Atmospheric Measurement Techniques 2019,* 12(9), 5019–5037, doi: 10.5194/amt-12-5019-2019.

Rose T, Crewell S, Löhnert U and Simmer CA. Network suitable microwave radiometer for operational monitoring of the cloudy atmosphere, *Atmospheric Research 2005,* 75(3), 183–200. doi: 10.1016/j.atmosres.2004.12.005.

Rückert JE, Walbröl A, Risse N, Krobot P, Haseneder-Lind R, Mech M, Ebell K and Spreen G. Microwave sea ice and ocean brightness temperature and emissivity between 22 and 243 GHz from ship-based radiometers, *Annals of Glaciology 2025*, 66:e8, 10.1017/aog.2025.1

Walbröl A, Crewell S, Engelmann R, Orlandi E, Griesche H, Radenz M, Hofer J, Althausen D, Maturilli M and Ebell K. Atmospheric temperature, water vapour and liquid water path from two microwave radiometers during MOSAiC, *Scientific Data 2022,* 9, 534, doi: 10.1038/s41597-022-01504-1.

Walbröl A, Griesche HJ, Mech M, Crewell S and Ebell K. Combining low- and high-frequency microwave radiometer measurements from the MOSAiC expedition for enhanced water vapour products, *Atmospheric Chemistry and Physics 2024*, 17(20), 6223-6245, doi: 10.5194/amt-17-6223-2024.